Geometric transition in friction for flow over a bubble mattress

Anthony M. J. Davis[a] and Eric Lauga[b]
Department of Mechanical and Aerospace Engineering, University of California San Diego, 9500 Gilman Drive, La Jolla, California 92093-0411, USA

(Received 20 October 2008; accepted 12 December 2008; published online 27 January 2009)

Laminar flow over a bubble mattress is expected to experience a significant reduction in friction since the individual surfaces of the bubbles are shear-free. However, if the bubbles are sufficiently curved, their protrusion into the fluid and along the flow direction can lead to an increase in friction as was recently demonstrated experimentally and computationally. We provide in this paper a simple model for this result. We consider a shear flow at low Reynolds number past a two-dimensional array of bubbles and calculate analytically the effective slip length of the surface as a function of the bubble geometry in the dilute limit. Our model is able to reproduce quantitatively the relationship between effective friction and bubble geometry obtained in numerical computations and, in particular, (a) the asymmetry in friction between convex and concave bubbles and (b) the existence of a geometric transition from reduced to enhanced friction at a critical bubble protrusion angle.
 [DOI: 10.1063/1.3067833]

Microfluidic devices are used to manipulate small volumes of liquids (micro- and nanoliters) and have important applications in biology, chemistry, and engineering.[1,2] However, from a practical standpoint, one important caveat of decreasing length scales is the increase in friction. For flow driven by a pressure gradient, ∇P, in a device of typical cross-sectional scale a, the volume flow rate scales as $Q \sim a^4 \nabla P/\eta$, where η is the viscosity of the fluid. Consequently, imposing a constant flow rate in a device decreasing in size requires a sharp increase in the applied pressure gradient as $\nabla P \sim 1/a^4$. For example, driving a flow rate of 1 μl of water per second in a 10 μm wide and 1 cm long device requires a pressure drop of many atmospheres.

Viscous friction is therefore an important issue on small scales, and engineers have looked for ways to reduce it. Recently a number of groups have reported slip, or apparent slip, for simple shear or pressure-driven flows over hydrophobic surfaces (see Refs. 3–5 for a review). Slip is typically characterized by a slip length λ, which is the fictional distance below the surface at which the velocity field would extrapolate to zero. For a shear flow with shear rate $\dot{\gamma}$ over a flat slipping surface, the velocity field is written as

$$\mathbf{u} = (\lambda \dot{\gamma} + \dot{\gamma} y)\hat{\mathbf{x}}, \tag{1}$$

where $\hat{\mathbf{x}}$ is the flow direction and y is the direction perpendicular to the surface. For a system of typical cross-sectional size a, friction decreases as some increasing function of λ/a.[3–9] Therefore for small enough systems, or large enough slip lengths, the friction reduction could be substantial. However, intrinsic slip lengths of hydrophobic surfaces do not exceed tens of nanometers.[3–5] As a result, the effect is small for devices on the micron scale, and other means of friction reduction must be devised.

One idea recently discussed is to exploit superhydrophobic surfaces[10,11] to reduce drag. When a hydrophobic solid surface [Fig. 1(a)] is sufficiently rough, under certain geometric conditions, a low-pressure high-surface-energy fluid in contact with the solid can spontaneously dewet,[11] thus transitioning from a Wenzel state where the fluid fills the grooves on the surface [Fig. 1(b)] to a fakirlike Cassie state where the fluid sits partially on the solid surface and partially on gas [Fig. 1(c)].[10,11] This phenomenon can also occur at the nanometer scale.[12] When dewetting does occur, shear stresses on the portion of the fluid interface in contact with the gas are expected to be insignificant, and the effective friction of such a superhydrophobic surface should be significantly lower than that of a solid surface. Drag reduction by superhydrophobic surfaces was indeed demonstrated experimentally both for macroscale pipe flow[13] as well as microchannels.[14,15] Numerical simulations also show a similar effect at the molecular scale.[12]

Liquids in contact with a mixed solid/gas interface are therefore expected to display low friction. However, one issue can potentially limit the drag-reducing properties of such surfaces, namely, the geometry of the gas-liquid interface. When the pressure in the gas is similar to that in the liquid above it, the interface remains flat [Fig. 1(d)], and drag is expected to be reduced by the gas-liquid interface. However, when the pressure in the gas is larger than that in the liquid, the interface becomes curved [Fig. 1(e)], with mean curvature given by the Young–Laplace equation.[11] In that case, the protrusion of the interface into the liquid curtails the drag-reducing properties of the surface by distorting the flow streamlines in the shear direction.[16–18] Notably, if we denote by θ the value of the protrusion angle of the spherical-cap interface with respect to the horizontal surface [see Fig. 1(e)], two recent experimental and numerical studies demonstrated that if the interface extends into the liquid beyond a critical value θ_c, the friction of the surface becomes larger than that of the original (flat) no-slip surface.[8,9] These results

[a]Electronic mail: amdavis@ucsd.edu.
[b]Electronic mail: elauga@ucsd.edu.

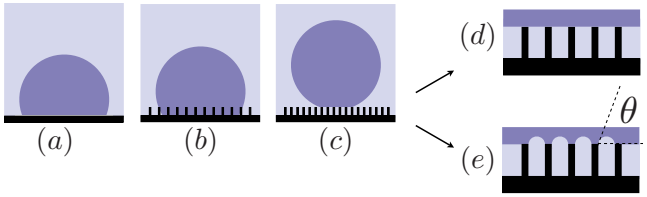

FIG. 1. (Color online) Superhydrophobic surfaces and bubble mattress: Liquid drop on a (a) flat hydrophobic surface, (b) rough hydrophobic surface in Wenzel state, and (c) rough hydrophobic surface in Cassie state. When the drops sit partially on air (Cassie state), the gas-liquid interface can be (d) flat or (e) curved, with a protrusion angle θ measured with respect to the horizontal direction.

imply therefore that the geometry of free surfaces plays a crucial role vis-à-vis the resistance to viscous flow, implying, in particular, that the recently discovered nanobubbles[19,20] might not always lead to as low a friction as previously thought.

Here, we specifically address this geometric transition from reduced to enhanced friction for shear flow over a collection of bubbles. We consider a simple two-dimensional model to predict the critical value of the apparent angle θ_c of the bubbles on the (otherwise) horizontal surface at which the effective surface starts displaying a friction larger than that obtained by a smooth solid surface. In the two-dimensional case, the velocity field can be solved exactly in the dilute limit, and the geometric transition is seen to happen at $\theta_c \approx 65°$. More generally the relationship between effective slip length and apparent angle from numerical simulations is well represented by our simple model.[8,9]

We consider therefore the setup displayed in Fig. 2: A dilute collection of two-dimensional bubbles (no-shear surfaces) on an otherwise no-slip surface. We assume the capillary number to be sufficiently small that the bubbles have perfectly circular shape. Their projected radius on the surface is c and they are separated by a distance $2L$. The bubble surface coverage is therefore given by $\phi = c/L$. The protrusion angle of the bubble into the fluid is denoted θ; $\theta > 0$ is a concave bubble that protrudes into the fluid [Fig. 2(b)],

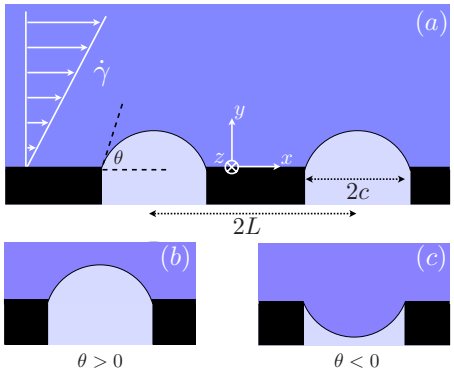

FIG. 2. (Color online) Setup for the two-dimensional calculation and notation: (a) shear flow (shear rate $\dot{\gamma}$) over a collection of bubbles of projected radius c, protrusion angle θ, and separation distance $2L$. The calculation is performed asymptotically in the dilute limit, $\phi = c/L \ll 1$; (b) the case $\theta > 0$ corresponds to a concave bubble protruding into the liquid; (c) $\theta < 0$ models a convex bubble curved away from the otherwise flat surface.

whereas $\theta < 0$ is a convex bubble protruding underneath the surface [Fig. 2(c)]. The velocity field away from the surface is a pure shear flow, with constant shear rate $\dot{\gamma}$. We denote by x the direction along the surface, y the direction of shear, and z the third direction and solve for the flow field in the limit of low Reynolds number.[21]

We first examine the case of a single bubble. The velocity field $\mathbf{v}$ is solved by introducing a stream function, $\mathbf{v} = \mathrm{curl}(\psi \hat{\mathbf{z}})$, where $\nabla^4 \psi = 0$ in the half-plane $y > 0$, indented by an arc of the circle $x^2 + (y + c \cot\theta)^2 = c^2 \csc^2\theta$ which perturbs the shear flow $\psi = \frac{1}{2}\dot{\gamma} y^2$. There is perfect slip without penetration at the surface of the two-dimensional bubble, and no slip is enforced at the rigid plane $y = 0$. We introduce toroidal coordinates defined by

$$x = \frac{c \sinh\xi}{\cosh\xi + \cos\eta}, \quad y = \frac{c \sin\eta}{\cosh\xi + \cos\eta}, \tag{2}$$

which is the conformal mapping $x + iy = c \tanh(\xi + i\eta)/2$. The fluid region is then $-\infty < \xi < \infty$, $\theta < \eta < \pi$, with $\xi = \pm\infty$ at the special points $(\pm c, 0)$, $\xi = 0$ on the y axis, $\eta = \theta$ on the arc, and $\eta = \pi$ at $y = 0$, $|x| > c$. A suitable biharmonic stream function, asymptotic at infinity to the prescribed shear flow, is given by[22,23]

$$\psi = \dot{\gamma} c^2 \left[\frac{\frac{1}{2}\sin^2\eta}{(\cosh\xi + \cos\eta)^2} - \frac{\int_0^\infty f(s,\eta)\cos s\xi \, ds}{\cosh\xi + \cos\eta} \right], \tag{3}$$

$$f = -A(s)\sin\eta \frac{\sinh s(\pi - \eta)}{s} + B(s)\left[\cos\eta \frac{\sinh s(\pi - \eta)}{s} + \sin\eta \cosh s(\pi - \eta) \right].$$

Here, two functions have been eliminated by imposing no slip ($\psi = 0 = \partial\psi/\partial\eta$ at $\eta = \pi$) on the rigid plane on either side of the bubble. Note that using the method in Eq. (3) allows us to capture the appropriate stress singularity at the contact point between the bubble and the surface.

The first equation for the functions A and B is established by demanding that the arc $\eta = \theta$ be a streamline on which $\psi = 0$. Thus the transform

$$\int_0^\infty \frac{\sinh s\eta}{\sinh s\pi} \cos s\xi \, ds = \frac{\frac{1}{2}\sin\eta}{(\cosh\xi + \cos\eta)} \quad (|\eta| < \pi) \tag{4}$$

yields, by substituting Eq. (3),

$$f(s,\theta) = \sin\theta \frac{\sinh s\theta}{\sinh s\pi}. \tag{5}$$

The second equation is established by demanding that the strain rate component $e_{\xi\eta}$ vanishes at $\eta = \theta$ in order to achieve perfect slip. Since

$$2e_{\xi\eta} = \frac{\partial}{\partial\xi}\left(-\frac{1}{h^2}\frac{\partial\psi}{\partial\xi} \right) + \frac{\partial}{\partial\eta}\left(\frac{1}{h^2}\frac{\partial\psi}{\partial\eta} \right), \tag{6}$$

$$h = \frac{c}{\cosh\xi + \cos\eta},$$

it is found that

$$\int_0^\infty \left[\frac{\partial^2 f}{\partial \eta^2} + (s^2+1)f\right]_{\eta=\theta} \cos s\xi ds$$
$$= \cos\theta\left[\frac{\cos\theta}{\cosh\xi + \cos\eta} + \frac{4\sin^2\theta}{(\cosh\xi+\cos\eta)^2}\right]$$
$$+ \sin\theta\left[-\frac{\sin\theta}{\cosh\xi+\cos\eta} + \frac{2\sin^3\theta}{(\cosh\xi+\cos\eta)^3}\right]. \quad (7)$$

The first and second derivatives of Eq. (4) give

$$\left[\frac{\partial^2 f}{\partial \eta^2} + (s^2+1)f\right]_{\eta=\theta} = \frac{2s[s\sin\theta\sinh s\theta + \cos\theta\cosh s\theta]}{\sinh s\pi}. \quad (8)$$

After substitution of Eq. (3) into Eq. (5) and Eq. (8), it is found that

$$A(s) = \frac{s}{\sinh 2s(\pi-\theta) + s\sin 2\theta} \times\left[\cos 2\theta + \frac{s\sin 2\theta\cosh s\pi + \sinh s(\pi-2\theta)}{\sinh s\pi}\right] \quad (9)$$

and

$$B(s) = \frac{s\sin 2\theta}{\sinh 2s(\pi-\theta) + s\sin 2\theta}. \quad (10)$$

We can now derive the result for a period array of bubbles. Away from the surface, the far-field velocity field is given, according to Eq. (2), by $\xi^2+(\pi-\eta)^2\to 0$ $(\eta<\pi)$, with

$$x \sim \frac{2c\xi}{\xi^2+(\pi-\eta)^2}, \quad y \sim \frac{2c(\pi-\eta)}{\xi^2+(\pi-\eta)^2}. \quad (11)$$

Hence the asymptotic form of the perturbation term in Eq. (3) is given by

$$2\dot{\gamma}c^2\frac{y^2}{x^2+y^2}\int_0^\infty A(s)ds. \quad (12)$$

In the presence of a periodic array of bubbles, with period $2L$, the prefactor in Eq. (12) is replaced by $\Sigma_{n=-\infty}^{\infty}\{y^2/[(x-2nL)^2+y^2]\}$ with a mean value available from the identity

$$\frac{1}{2L}\int_{-L}^{L}\sum_{n=-\infty}^{\infty}\frac{y^2dx}{(x-2nL)^2+y^2} = \frac{y}{2L}\int_{-\infty}^{\infty}\frac{ydx}{x^2+y^2} = \frac{\pi y}{2L}. \quad (13)$$

Consequently, the far-field velocity perturbation is given by

$$\pi\dot{\gamma}c\left(\frac{c}{L}\right)\int_0^\infty A(s)ds\hat{\mathbf{x}}, \quad (14)$$

which, with $A(s)$ given by Eq. (9), is identified as an effective slip speed at $y=0$ with dimensionless slip length [see Eq. (1)],

$$\frac{\lambda}{c} = \pi\left(\frac{c}{L}\right)\int_0^\infty A(s)ds. \quad (15)$$

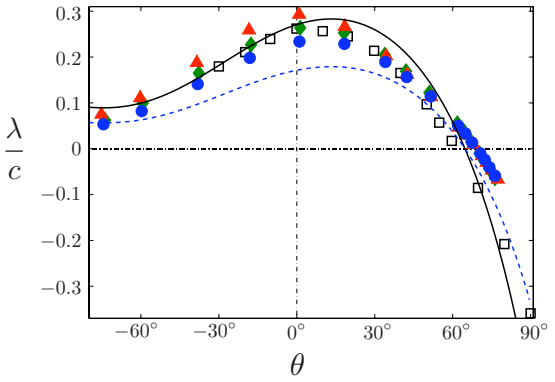

FIG. 3. (Color online) Comparison between the numerical data of Ref. 8 (empty symbols) and Ref. 9 (filled symbols) and our two-dimensional dilute model: Dimensionless effective slip length as a function of the protrusion angle of the bubble into the fluid. Symbols: Square lattice [□, ϕ=0.68 (Ref. 8; ●, ϕ=0.43 (Ref. 9)]; rectangular lattice [◆, ϕ=0.43 (Ref. 9)]; rhombic lattice [▲, ϕ=0.43 (Ref. 9)]. Lines: Our two-dimensional dilute model, Eq. (15), for two different surface coverages, ϕ=0.43 (- - -) and ϕ=0.68 (—).

Let us now compare the predictions of our model [Eq. (15)] with the numerical computations of Refs. 8 and 9. The results are displayed in Fig. 3, where we plot the effective slip length of the surface (nondimensionalized by the projected bubble radius on the surface, c) as a function of the protrusion angle θ into the fluid. The simulations of Ref. 8 consider a three-dimensional square lattice, with a surface coverage of the bubbles ϕ=0.68 (squares). The computations of Ref. 9 are for three different lattices (square lattice, circles; rectangular lattice, lozenges; rhombic lattice, triangles) and in all cases where the dependence on the protrusion angle is studied the fraction of the surface covered by the bubbles is ϕ=0.43. We also plot in Fig. 3 the results of our model for both surface coverage considered in the two previous studies: ϕ=0.43 (dashed line) and ϕ=0.68 (solid line).[24]

The main features of the full numerical results are seen to be reproduced by our analytical model. There exists a critical protrusion angle θ_c above which the effect of the wall-attached bubbles displays a transition from reduced $(\theta<\theta_c)$ to enhanced friction $(\theta>\theta_c)$. Our model predicts $\theta_c\approx 65°$, in good agreement with the results of Ref. 8 $(\theta_c\approx 62°)$ and Ref. 9 $(\theta_c\approx 69°)$. Our model also successfully reproduces the asymmetry in the friction curves between $\theta<0$ and $\theta>0$, indicating a qualitative difference between the effect of convex and concave bubbles on shear flow. Experimentally, this asymmetry implies that flow over an array of bubbles at a lower pressure than the fluid $(\theta<0)$ is less likely to show an increase in wall friction than flow over an array of bubbles with a larger pressure than the fluid $(\theta>0)$.

The model we consider here is two dimensional. A simple argument can also be made to show that the critical protrusion angle lies in the range $0°<\theta_c<90°$ in three dimensions. For θ=0°, the bubbles are flat disks, for which the calculation is available in Ref. 25, where it is found[26] that the asymptotic form of the perturbation flow component v_x is $2\dot{\gamma}c^3yx^2/3\pi r^5$, with $r^2=x^2+y^2+z^2$. In the presence of a (di-

lute) square lattice of such disks, with period $2L$, the effective slip length is simply found to be $\lambda/c=c^2/9L^2$. This is the same result as that obtained by Ref. 6 and indicates that bubbles with $\theta=0°$ reduce the effective friction of the surface, and therefore $0° < \theta_c$. In the case where $\theta=90°$ (hemispherical bubble), the velocity field is readily verified to be given by $\mathbf{v}=\dot{\gamma}y[\hat{\mathbf{x}}-c^3x\hat{\mathbf{r}}/r^4]$.[18,27] In the presence of a square lattice of such bubbles, the perturbation velocity in the far field can be simply added up (in the dilute limit), and the obtained slip length is given by $\lambda/c=-\pi c^2/6L^2$. The negative slip length indicates that the array of stress-free hemispheres increases the effective friction of these surfaces, and therefore $\theta_c < 90°$.

In summary, this paper presents a two-dimensional model of shear flow past an array of bubbles. We calculate the effective slip length of the surface in the dilute limit and find good agreement with recent numerical three-dimensional numerical simulations for flow over superhydrophobic surfaces. In particular, our results reproduce the asymmetry between convex and concave bubbles, as well as the existence of a geometric transition from low to high friction at a critical bubble protrusion angle. Our approach provides therefore the minimal model necessary to quantitatively capture the interplay between low friction and geometry in shear flows.

Our results could be extended by relaxing the various assumptions made in the paper, in particular, by going beyond the two-dimensional, dilute, and zero capillary number limits. In the case of three-dimensional bubbles, the issue of geometry of the lattice needs to be further explored as well. Experimentally, the fabrication of controlled porous surfaces[28] or predesigned bubble lattices[29] would present exciting opportunities to map out and optimize the frictional properties of superhydrophobic surfaces. In addition, simulations showing an increase in friction of a bubble mattress with capillary numbers[9] could be addressed with a similar framework.

This work was supported in part by the National Science Foundation (Grant Nos. CTS-0624830 and CBET-0746285).

[1] H. A. Stone, A. D. Stroock, and A. Ajdari, "Engineering flows in small devices: Microfluidics toward a lab-on-a-chip," Annu. Rev. Fluid Mech. **36**, 381 (2004).
[2] T. M. Squires and S. R. Quake, "Microfluidics: Fluid physics on the nanoliter scale," Rev. Mod. Phys. **77**, 977 (2005).
[3] C. Neto, D. R. Evans, E. Bonaccurso, H.-J. Butt, and V. S. J. Craig, "Boundary slip in Newtonian liquids: A review of experimental studies," Rep. Prog. Phys. **68**, 2859 (2005).
[4] E. Lauga, M. P. Brenner, and H. A. Stone, "Microfluidics: The no-slip boundary condition," *Handbook of Experimental Fluid Dynamics*, edited by A. Y. C. Tropea and J. F. Foss (Springer, New York, 2007).
[5] L. Bocquet and J.-L. Barrat, "Flow boundary conditions: From nano-to micro-scales," Soft Matter **3**, 685 (2007).
[6] M. Sbragaglia and A. Prosperetti, "Effective velocity boundary condition at a mixed slip surface," J. Fluid Mech. **578**, 435 (2007).
[7] C. Ybert, C. Barentin, C. Cottin-Bizonne, P. Joseph, and L. Bocquet, "Achieving large slip with superhydrophobic surfaces: Scaling laws for generic geometries," Phys. Fluids **19**, 123601 (2007).
[8] A. Steinberger, C. Cottin-Bizonne, P. Kleimann, and E. Charlaix, "High friction on a bubble mattress," Nature Mater. **6**, 665 (2007).
[9] J. Hyvaluoma and J. Harting, "Slip flow over structured surfaces with entrapped microbubbles," Phys. Rev. Lett. **100**, 246001 (2008).
[10] D. Quere, "Non-sticking drops," Rep. Prog. Phys. **68**, 2495 (2005).
[11] P.-G. de Gennes, F. Brochard-Wyart, and D. Quéré, *Capillarity and Wetting Phenomena: Drops, Bubbles, Pearls, Waves* (Springer, New-York, 2004).
[12] C. Cottin-Bizonne, J. L. Barrat, L. Bocquet, and E. Charlaix, "Low-friction flows of liquid at nanopatterned interfaces," Nature Mater. **2**, 237 (2003).
[13] K. Watanabe, Y. Udagawa, and H. Udagawa, "Drag reduction of Newtonian fluid in a circular pipe with a highly water-repellent wall," J. Fluid Mech. **381**, 225 (1999).
[14] J. Ou, B. Perot, and J. P. Rothstein, "Laminar drag reduction in microchannels using ultrahydrophobic surfaces," Phys. Fluids **16**, 4635 (2004).
[15] J. Ou and J. P. Rothstein, "Drag reduction and μ-PIV measurements of the flow past ultrahydrophobic surfaces," Phys. Fluids **17**, 103606 (2005).
[16] S. Richardson, "On the no-slip boundary condition," J. Fluid Mech. **59**, 707 (1973).
[17] K. M. Jansons, "Determination of the macroscopic (partial) slip boundary condition for a viscous flow over a randomly rough-surface with a perfect slip microscopic boundary condition," Phys. Fluids **31**, 15 (1988).
[18] D. Legendre and C. Colin, "Enhancement of wall-friction by fixed cap-bubbles," Phys. Fluids **20**, 051704 (2008).
[19] N. Ishida, T. Inoue, M. Miyahara, and K. Higashitani, "Nano bubbles on a hydrophobic surface in water observed by tapping-mode atomic force microscopy," Langmuir **16**, 6377 (2000).
[20] J. W. G. Tyrrell and P. Attard, "Images of nanobubbles on hydrophobic surfaces and their interactions," Phys. Rev. Lett. **87**, 176104 (2001).
[21] J. Happel and H. Brenner, *Low Reynolds Number Hydrodynamics* (Prentice-Hall, Englewood Cliffs, 1965).
[22] A. M. J. Davis and M. E. O'Neill, "Separation in a stokes flow past a plane with a cylindrical ridge or trough," Q. J. Mech. Appl. Math. **30**, 355 (1977).
[23] P. M. Morse and H. Feshbach, *Methods of Theoretical Physics* (McGraw-Hill, New York, 1953), Vol. II.
[24] Strictly speaking, our two-dimensional model was derived in the low-ϕ limit. We consider, however, its results beyond its regime of asymptotic validity, as it is expected to provide a good quantitative model even in the limit of large ϕ and reproduce the essentially physical features of the phenomenon.
[25] A. M. J. Davis, "Shear flow disturbance due to a hole in the plane," Phys. Fluids A **3**, 478 (1991).
[26] After noting that, in Eq. (22) of Ref. 25, the toroidal coordinate $\lambda \sim r$ in the far field and $\zeta=y/\lambda$.
[27] D. Legendre, C. Colin, and T. Coquard, "Lift, drag and added mass of a hemispherical bubble sliding and growing on a wall in a viscous linear shear flow," Philos. Trans. R. Soc. London, Ser. A **366**, 2233 (2008).
[28] Y. M. Zheng, L. Jiang, J. X. Wang, and D. Han, "Extreme "water repellency" on strong water-spreading surface without tilted degree actuation," Appl. Phys. Lett. **93**, 094107 (2008).
[29] N. Bremond, M. Arora, C. D. Ohl, and D. Lohse, "Controlled multibubble surface cavitation," Phys. Rev. Lett. **96**, 224501 (2006).